Kovove Mater. 50 2012 169–175
DOI: 10.4149/km_2012_3_169

Effect of nano-Y_2O_3 on microstructure and diffusive behavior of Ti_3Al/Al_3Ti matrix composite coatings

J. N. Li[1], H. J. Yu[2], C. Z. Chen[1]*, W. Li[1]

[1]*Key Laboratory for Liquid-Solid Structural Evolution and Processing of Materials (Ministry of Education), Department of Materials Science, Shandong University, Jinan 250061, Jing Shi Road # 17923, Shandong, China*
[2]*School of Mechanical Engineering, Shandong Unversity, Jinan 250061, China*

Received 29 July 2011, received in revised form 27 October 2011, accepted 2 November 2011

Abstract

Laser cladding of the Al_3Ti+TiC+(Ni-coated WC) pre-placed powders on titanium alloy can form the Ti_3Al/Al_3Ti matrix composite coating, which improves the surface performance of the substrate. With addition of nano-Y_2O_3, this composite coating exhibited a finer microstructure. In this study, the Al_3Ti+TiC+(Ni-coated WC)+nano-Y_2O_3 laser-cladded coatings have been researched by means of X-ray diffraction and scanning electron microscope. The function of nano-Y_2O_3 acted as the heterogeneous nuclei, and the growth of the grains was hindered by Y_2O_3 and Y. Y_2O_3 can also decrease the temperature of the molten pool. Thus, the probability that grains traverse potential barrier decreased, leads to more stability of the grains.

K e y w o r d s: coatings, rare earth compounds, laser cladding, intermetallics, diffusion

1. Introduction

Laser cladding is a rapid-solidification process, which can greatly improve the wear resistance of the titanium alloys. Carbide metals are known for a high resistance to all types of wear [1]. Compared to the other carbides, WC combine favorable properties, such as high hardness, high density and a good wettability with molten bonding metals.

Laser cladding reinforced coating on metal surface is an available surface modification technique, which was developed in recent years. Nevertheless, the application of the laser cladding was not widely enough due to the unavoidable cracks or other defects in the cladding layer. Nano-materials have strong acoustic, optic, electric, magnetic and thermodynamic characteristics because of their quantum size and surface effect. In the field of surface engineering, nano-materials have been found in the research reports on spraying and laser surface alloy, etc. [2, 3]. In the field of surface engineering, nano-Y_2O_3 can further refine the microstructures of the laser-cladded coatings, and also reduce the tendency of cracking [4, 5]. Moreover, rare earth oxide reinforced metal matrix composites have potential application in the aerospace industry. Through the experiment, it was found that Al_3Ti was suitable to be used as the laser cladding powder. During the cladding process, a portion of Al_3Ti was able to react with Ti, leading to the formation of Ti_3Al, which also showed high micro-hardness and good wear resistance.

In this paper, the effect of nano-Y_2O_3 on microstructures and phase constituents of the Al_3Ti+TiC+(Ni-coated WC) laser-cladded coating is introduced. This research provided essential experimental and theoretical basis to promote the application of the laser cladding technique in the manufacturing and the repairing of the aerospace parts.

2. Experimental

A 1.5 kW continuous wave CO_2 laser, with a beam diameter of 4 mm, was employed to melt the surface of the samples. During the laser cladding process, the powders were dissolved into the melted pool. During

*Corresponding author: tel./fax: +86 531 88395991; e-mail address: czchen@sdu.edu.cn

Table 1. The parameters and the materials of laser cladding process in the experiment

Number	Substrate materials	Powders composition (wt.%)	Laser power (W)	Scanning speed ($mm\,s^{-1}$)	Spot diameter (mm)
Sample 1	Ti-6Al-4V alloy	Al_3Ti + 30TiC + 15(Ni-coated WC)	850–1200	2.5–5	4
Sample 2		Al_3Ti + 30TiC + 35(Ni-coated WC)			
Sample 3		Al_3Ti + 30TiC + 35(Ni-coated WC) + 1.5 nano-Y_2O_3			

the laser cladding process, surface oxidation was prevented by inert gas (Ar) with the flowing rate of 30 $l\,min^{-1}$.

The materials used in this experiment were Ti-6Al-4V alloy and the pre-placed powders of Al_3Ti ($\geq$ 99.5 % purity, 150–250 μm), TiC ($\geq$ 98.5 % purity, 100–250 μm), Ni-coated WC ($\geq$ 99.5 % purity, 50–100 μm, 15 wt.% Ni) and Y_2O_3($\geq$ 99.5 % purity, 10–200 nm) for the laser cladding, and the thickness of the pre-placed coating was 0.6–0.8 mm. The size of the Ti-6Al-4V alloy (6 wt.% Al, 4 wt.% V, $\leq$ 0.3 wt.% Fe, $\leq$ 0.1 wt.% C, $\leq$ 0.15 wt.% Si, $\leq$ 0.2 wt.% O, balance Ti) was 10 mm × 10 mm × 10 mm. It should be mentioned that too high power can burn out a portion of the pre-placed powders, which can greatly influence the quality of the coatings. Reversely, the laser power induced the inter-diffusion of substrate material to cladded material, and the laser surface alloying can not occur completely with too low power. Hence, the power was in the range of 850–1000 W. During the cladding process, the parameters of these three samples were the same. The parameters and the materials of the experiment are shown in Table 1.

The samples were polished and etched in a hydrofluoric acid + nitric acid aqueous solution. The volume ratio of hydrofluoric acid, nitric acid and aqueous solution was 1 : 2 : 3. DMAX/2500PCX X-ray diffraction (XRD) was used to determine the phase constitutes of the laser-cladded coatings. The microstructural morphologies of the coatings were analyzed by means of QUANTA200 scanning electron microscope (SEM). The elements distributions of the coatings were measured using JXA-880R electron probe micro-analyzer (EPMA).

3. Results and analysis

3.1. Microstructure of Al_3Ti+TiC+(Ni-coated WC) laser-cladded coating

As is shown in Fig. 1a, there was a metallurgical combination between the coating of sample 2 and the Ti-6Al-4V alloy substrate, and the α-Ti acicular martensite was obviously present in the interface zone. The presence of α-Ti acicular martensite can greatly improve the ductility of the titanium alloys at room temperature. Moreover, the bulk-shape precipitates were present in the clad zone. The surface of this coating was not smooth, and there were protuberant block-shape precipitates adjacent on it (Fig. 1b). It was known that the melting point of TiC (3420 ℃) was higher than that of WC (2870 ± 50 ℃). Thus, during the freezing time, TiC precipitated firstly from the molten pool, then WC precipitated around it. It was found that a number of the precipitates were present in the interface zone of coating of sample 2 (Fig. 1a). However, few of the precipitates were produced in the interface zone of sample 1 (Fig. 1c). It is reasonable that with the decrease of the WC content, less WC phases were able to grow up primarily and precipitated around TiC. Moreover, it was known that the density of WC (15.63 $g\,cm^{-3}$) was significantly higher than that of TiC (4.93 $g\,cm^{-3}$). Thus, it can be speculated that the density of the precipitates in coating of sample 2 was higher than that of sample 1 due to the action of the high content of the WC protuberant precipitates. Therefore, according to Fig. 1c, it can be deduced that the precipitates of sample 1 have a very marked trend to float on the surface of molten pool during the solidification process.

As is shown in Fig. 1c,d, the microstructure of the coating in sample 1 was eutectic γ-Ni, and was in cell and cell-dendrite morphologies. Furthermore, it was also found that the fine size spherical WC precipitates were present in this coating. In fact, when cooling and solidification started, the partially melted WC particles provided the nuclei for heterogeneous nucleation and grew up into the spherical precipitate in shapes related to local composition and temperature gradient [6]. However, the WC precipitates had very limited time to grow up due to the rapid supercooling rate in molten pool, thus resulting in the fine size (Fig. 1d).

3.1.1. EPMA analysis

Electron probe micro-analyzer (EPMA) line scan results showed the distributions of the Ti, Al, W and C elements in coating of sample 2 (Fig. 2a). It was noticed that when the precipitate was scanned, the peaks of Ti and C decreased. Moreover, the diffraction peak of W was highest in the protuberant block-shape precipitates (Fig. 2b). Thus, it was considered that the

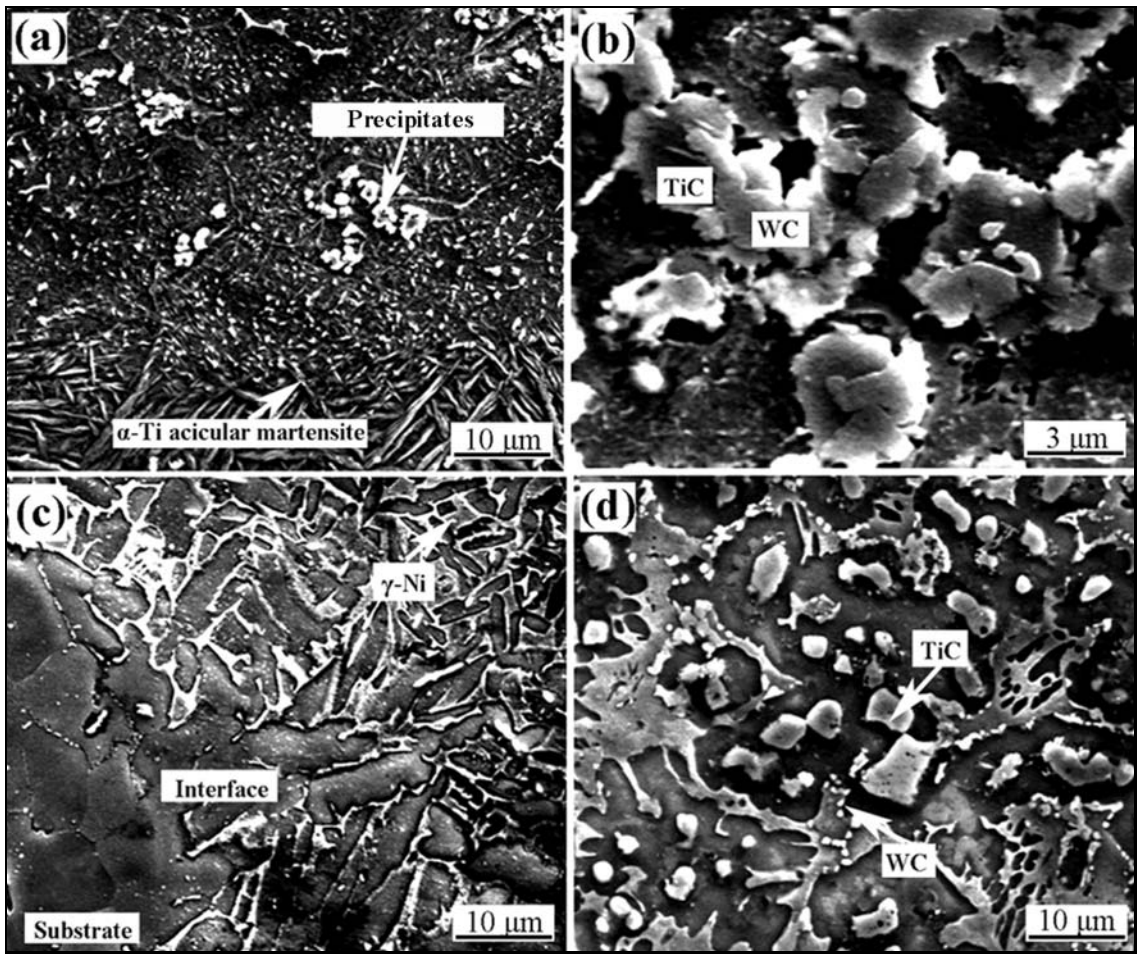

Fig. 1. SEM micrographs of the coatings in samples 1 and 2: (a) the interface zone (sample 2), (b) the TiC and WC precipitates (sample 2), (c) the interface zone (sample 1), (d) the clad zone (sample 1).

protuberant precipitate mainly consisted of WC, and the bulk-shape precipitates below it were TiC. On the other hand, it was noted that the diffraction peaks of Ti and Al in the matrix of the coating were uniform. Combining the XRD results, it was considered the matrix of the coating mainly consisted of Ti_3Al and Al_3Ti. Furthermore, there were also weak diffraction peaks of C and W in the matrix. It was proved that after laser cladding, a portion of the WC pre-placed powder dissolved into the matrix of the coating.

3.2. XRD analysis

The overlap of XRD patterns of the coatings surface of sample 1, 2 and 3 illustrated a significant phase evolution after the laser cladding. As is shown in Fig. 3, it was found out that the phase area of the coating surface of sample 1 consisted of γ-Ni, Al_3Ti, Ti_3Al, TiC, WC and WC_x. In fact, during the cladding process, a large amount of liquid Ti entered into the molten pool from the substrate due to the dilution action, which could further react with Al_3Ti, leading to the formation of Ti_3Al.

The XRD results revealed that the matrix of the coating in sample 2 mainly consisted of γ-Ni and Al_3Ti/Ti_3Al. Moreover, according to the EPMA results, there were also W and C in the matrix of the coating. It was considered that during the cladding process, the WC powders might partially melt into the matrix of the coating, then mix with TiC, eutectic γ-Ni and liquid Al_3Ti/Ti_3Al. This process greatly increased the density of the liquid in the molten pool, and was also favorable to the production of WC_x.

In addition, the TiC diffraction peak of the coating in sample 2 was significantly lower than that of sample 1. As mentioned previously, with the increasing of the WC mass fraction, more WC precipitates were produced around TiC, which forced the precipitates to sink down into the bottom of the molten pool, thus resulting in the lower diffraction peak [7]. However, it is interesting to note that with addition of

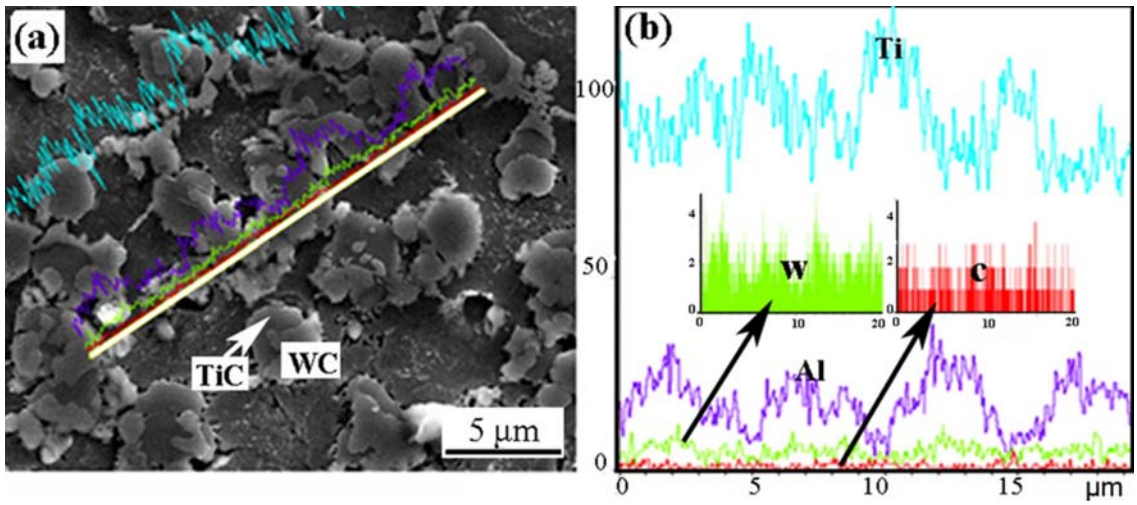

Fig. 2. EPMA line scan results of the coating in sample 2: (a) the clad zone, and (b) Ti, Al, W and C.

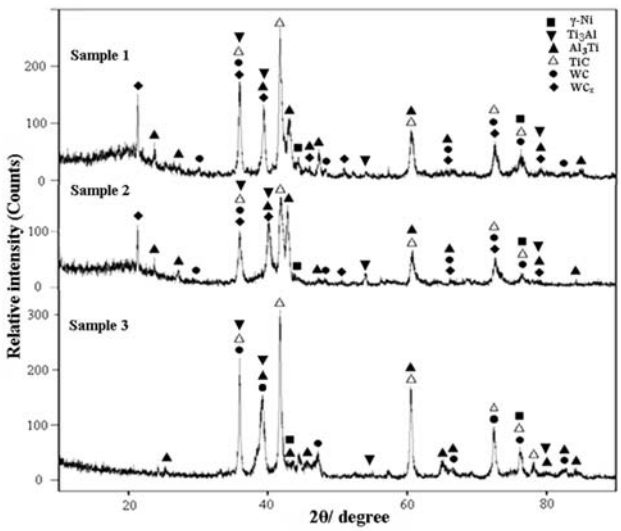

Fig. 3. X-ray diffraction diagrams of the coatings in samples 1, 2 and 3.

nano-Y_2O_3, the diffraction peak of TiC in sample 3 was higher than that of sample 1. Qu et al. reported [8] that nano-Y_2O_3 suppressed the crystallization and growth of the WC crystals in a certain extent. Therefore, a portion of WC was not able to be precipitated around the TiC precipitate. As a result, a large amount of the TiC precipitates had a trend to float on the surface of the molten pool, leading to the enhancement of the TiC diffraction peak. It was also noted that WC_x was not present in the XRD pattern of sample 3. In fact, during the cladding process, a portion of added Y_2O_3 decomposed and released atomic Y as follows [9]:

$$2Y_2O_3 \rightarrow 4Y + 3O_2 \uparrow . \quad (1)$$

In addition, a portion of TiC delivered Ti and C atoms into the molten pool. Y can greatly reduce activity of the C particles, which hindered the reaction between C and WC in a certain extent [10]. Thus, WC_x was not produced in the coating of sample 3.

3.3. *Microstructure of $Al_3Ti+TiC+$(Ni-coated WC)$+Y_2O_3$ coating*

As was shown in Fig. 4a, it was noted that the precipitates of the coating in sample 3 exhibited a smooth surface free of the protuberant precipitates. Combining the energy dispersive spectrometer (EDS) spectrum analysis of the bulk-shape precipitates ensured that only TiC was located in it. In fact, during the solidification process, Y_2O_3 was likely to grow in sphericity due to its c-style RE_2O_3 crystal structure (Fig. 4b). Consequently, the solidified nano-Y_2O_3 fine grains gone on growing in front of precipitates and prevented the growth of them. Hence, the average size of the TiC precipitations in coating of sample 3 was finer than that of sample 2. In fact, once the molten layer formed, the dispersoids dissolved partially or fully, and hence, nano-Y_2O_3 can neither remain Y_2O_3 nor nanometric in size. However, the energy distribution of the laser beam was uneven. Thus, a portion of the nano-Y_2O_3 particles in the edge of facula were able to retain the nano-metric size, which diffused into every location of the molten pool due to their high diffusion coefficient [11]. As is shown in Fig. 4b, some Y_2O_3 reinforcements with nanometer sizes existed in the coatings. It was also noted that an agglomeration of the Y_2O_3 nano-particles was present in the coating (Fig. 4d), this indicated that nano-Y_2O_3 could be easily reunited because of the surface effect. The agglomeration of nano-Y_2O_3 particles was generally located on the grain boundaries, which suppressed the crystallization and growth of the WC crystal (Fig. 4c)

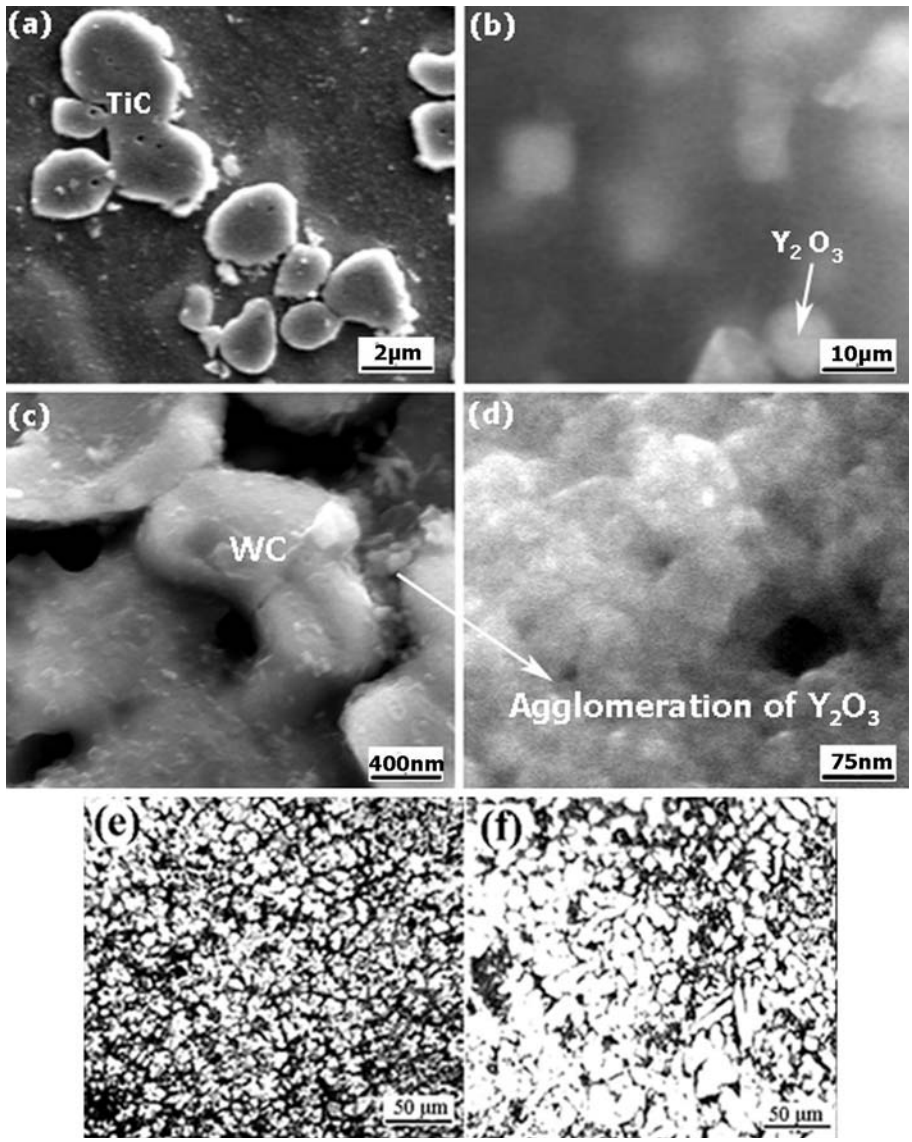

Fig. 4. SEM micrographs of the composite coatings in sample 3: (a) the TiC precipitates, (b) nano-Y_2O_3, (c) the WC crystals, (d) agglomeration of nano-Y_2O_3, (e) coating in sample 3, and (f) coating in sample(2).

[12]. Therefore, the WC precipitates were not present in the coating in sample 3.

As is shown in Fig. 4e,f, the microstructure of coating in sample 3 was finer than that of sample 2. It is known that nano-Y_2O_3 was effective in grain refinement, which acted as heterogeneous nucleation sites in clad zone, so the growth of dendrites was restricted by forming more nuclei, thus resulting in the compacter and finer microstructure [13]. Moreover, it should be mentioned that adding nano-Y_2O_3 to the coating was beneficial in decreasing amounts of vacancies condensed at the composite grain boundaries, and also reducing the internal stress of the laser-cladded coating, which prevented the production of the micro--crack in coating.

As mentioned previously, the WC_x diffraction peak was not present in the XRD pattern of sample 3. It can be speculated that a vast amount of the kinetic process in the solid and liquids states deals with mass transport limited by the potential barriers [14]. During the laser cladding process, the potential barrier acted as barriers against carrier transportation and as preferential sites for the electron-hole or the particles-hole recombination [15]. Therefore, if the C particles intended to jump into the other site, leading to formation of WC_x, they should traverse the potential barrier first.

We can write the Schrodinger equation as follows:

$$\nabla^2\psi + k^2(x)\psi = 0, \tag{2}$$

$$k(x) = \frac{1}{\hbar}\sqrt{2m[E - V(x)]}, \tag{3}$$

where V is the potential energy and $\hbar$ is the Planck constant, E is the energy of the C particles, ψ is

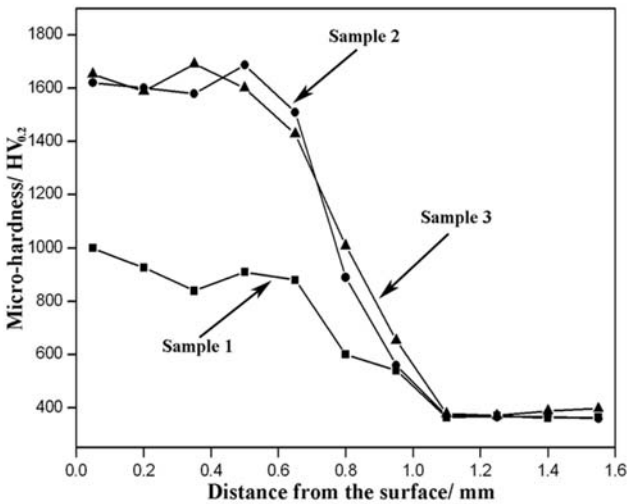

Fig. 5. The micro-hardness distributions of the composite coatings in samples 1, 2 and 3.

the wave function, m is the particle's mass. Furthermore, P is the momentum of the particles, $P = \sqrt{2m[E - V(x)]} = \hbar k$. If $E > V(x)$, the particles are able to traverse the potential barrier easily. It is known that for harmonic oscilator $E = \hbar(n + 1/2)\omega$, where ω is the angular velocity of vibration of the nearest-neighbor to the point vacancy. In addition, it is supposed that the height of the potential barrier is E_1. According to the Boltzmann statistical distribution, at temperature T, the probability that the C particles have the energy E_1 is proportional to the Boltzmann factor as follows [16]:

$$p(E_1) \sim \mathrm{e}^{-E_1/k_\mathrm{B}T}. \tag{4}$$

Hence, it can be deduced that with decreasing temperature, the probability that the atom traverses the potential barrier is decreasing. It is known than the energy can be released during the process of the crystallization of WC. According to the principle mentioned previously, nano-Y_2O_3 hinders the crystallization of WC, thus resulting in decrease of temperature in the molten pool of sample 3. Therefore, it was considered that with decreasing temperature, few of the C particles were able to traverse the potential barrier, which resulted in disappearance of WC_x. This principle may also explain the phenomenon of the agglomeration of nano-Y_2O_3.

3.4. Micro-hardness

It was found that the micro-hardness of the coating in sample 1 was in the range of 800–1000 $HV_{0.2}$, which is approximately 2–3 times higher than that of Ti-6Al-4V alloy substrate (about 360 $HV_{0.2}$) mainly due to the action of the Al_3Ti/Ti_3Al + WC/TiC phases. The micro-hardness of the coating in sample 2 was in the range of 1550–1700 $HV_{0.2}$, and the micro-hardness of the coating in sample 3 was also in this range (Fig. 5). It was considered that nano-Y_2O_3 hindered the crystallization and growth of the WC crystals in a certain extent. Thus, the micro-hardness of the coating in sample 3 should be decreased as it was free of the WC dispersions. Nevertheless, as mentioned previously, nano-Y_2O_3 hindered the movement of the dislocation and also refined the microstructure of the coating, which was beneficial in increasing the micro-hardness of the coating. Hence, the micro-hardness distributions of samples 2 and 3 were similar.

4. Conclusions

During the laser cladding process, the addition of nano-Y_2O_3 decreased the temperature of the molten pool, and also decreased the probability that the grains traversed the potential barrier, thus resulting in more stability of the grains. Laser cladding of the Al_3Ti+TiC+(Ni-coated WC) pre-placed coating on the Ti-6Al-4V alloy can form the coating with a metallurgical combination to substrate, which increases greatly the micro-hardness and wear resistance of the Ti-6Al-4V alloy. The matrix of the coating mainly consisted of γ-Ni, Al_3Ti/Ti_3Al and WC_x, and the TiC/WC precipitates were dispersed on the matrix. Nano-Y_2O_3 prevented the production of the WC_x/WC precipitates in the Al_3Ti+TiC+(Ni-coated WC) laser-cladded coating in a certain extent. The function of nano-Y_2O_3 acted as heterogeneous nuclei, and the growth of the grains was hindered by Y_2O_3 and Y. With addition of nano-Y_2O_3, the coating exhibited the compact and fine microstructure.

Acknowledgements

This work was financially supported by the Department of Science and Technology of Jinan, Shandong Province (Grant No. [2006]060166), P. R. China.

References

[1] Przybylowicz, J., Kusinski, J.: J. Mater. Process. Technol., *109*, 2001, p. 154. doi:10.1016/S0924-0136(00)00790-1
[2] Hajiesmaeibaigi, F., Motamedi, A., Ruzbehani, M.: Laser Phys., *20*, 2010, p. 508. doi:10.1134/S1054660X10030072
[3] Emel'yanov, V. I.: Laser Phys., *8*, 2008, p. 682.
[4] Besterci, M., Šlesár, M., Sulleiová, K., Zbíral, J.: Kovove Mater., *39*, 2001, p. 422.
[5] Besterci, M., Šlesár, M., Ivan, J., Zbíral, J.: Kovove Mater., *35*, 1997, p. 13.

[6] Zhong, M. L., Liu, W. J., Yao, K. F., Goussain, J. C., Mayer, C., Becker, A.: Surf. Coat. Technol., *157*, 2002, p. 128. doi:10.1016/S0257-8972(02)00165-2
[7] Przybylowicz, J., Kusinski, J.: J. Mater. Process. Technol., *109*, 2001, p. 154. doi:10.1016/S0924-0136(00)00790-1
[8] Qu, N. S., Zhu, D., Chan, K. C.: Scripta Mater., *54*, 2006, p. 14215. doi:10.1016/j.scriptamat.2005.10.069
[9] Tian, Y. S., Chen, C. Z., Chen, L. X., Huo, Q. H.: Scripta Mater., *54*, 2006, p. 8472.
[10] Yao, Y. W., Yao, S. W., Zhang, L., Wang, H. Z.: Mater. Lett., *61*, 2007, p. 67. doi:10.1016/j.matlet.2006.04.007
[11] Li, J. N., Chen, C. Z., Zhang, C. F., Li, W.: Mater. Res. Innovations, *15*, 2011, p. 344. doi:10.1179/1433075X11Y.0000000008
[12] Zhou, Y., Peng, X., Wang, F.: Scripta Mater., *55*, 2006, p. 1039. doi:10.1016/j.scriptamat.2006.08.004
[13] Vilar, R., Santos, E. C., Ferreira, P. N., Franco, N., da Silva, R. C.: Acta Mater., *57*, 2009, p. 5292. doi:10.1016/j.actamat.2009.06.049
[14] Adamczyk, Z.: J. Colloid Interface Sci., *229*, 2000, p. 477. PMid:10985827. doi:10.1006/jcis.2000.6993
[15] Idrish Miah, M., Gray, E. M.: Curr. Opin. Solid State Mater. Sci., *13*, 2009, p. 99. doi:10.1016/j.cossms.2009.02.002
[16] Sinno, T.: J. Cryst. Growth, *303*, 2007, p. 5. doi:10.1016/j.jcrysgro.2006.11.278